frontiers | Frontiers in Mechanical Engineering

TYPE Methods
PUBLISHED 14 June 2024
DOI 10.3389/fmech.2024.1414626

OPEN ACCESS

EDITED BY
Kai Wang,
Hunan University, China

REVIEWED BY
Dongguo Tan,
Hunan University of Science and Technology, China
Yunlong Chang,
Shenyang University of Technology, China

*CORRESPONDENCE
Thanh-Hai Nguyen,
haint@hcmut.edu.vn

RECEIVED 09 April 2024
ACCEPTED 23 May 2024
PUBLISHED 14 June 2024

CITATION
Tran-The Chung V, Thi-Minh Tran Q, Nguyen N-H, Ha-Quang Ngo T, Le T-K and Nguyen T-H (2024), Optimization of tempering temperature and soaking time of SCM440 steel horn in ultrasonic-assisted metal inert gas welding.
Front. Mech. Eng 10:1414626.
doi: 10.3389/fmech.2024.1414626

Optimization of tempering temperature and soaking time of SCM440 steel horn in ultrasonic-assisted metal inert gas welding

Vinh Tran-The Chung[1,2,3], Quynh Thi-Minh Tran[1,2], Ngoc-Ha Nguyen[1,2], Thinh Ha-Quang Ngo[1,2], Trung-Kien Le[4] and Thanh-Hai Nguyen[1,2]*

[1]Faculty of Mechanical Engineering, Ho Chi Minh City University of Technology (HCMUT), Ho Chi Minh City, Vietnam, [2]Viet Nam National University Ho Chi Minh City, Ho Chi Minh City, Vietnam, [3]Ly Tu Trong College, Ho Chi Minh City, Vietnam, [4]School of Mechanical Engineering, Hanoi University of Science and Technology, Hanoi, Vietnam

This study explores the optimization of ultrasonic horn heat treatment conditions for enhanced mechanical quality (Q_m). The optimal parameters identified are a tempering temperature of 529°C and a 240-min soaking time, yielding a 1.3% experimental error. Frequency stability during welding is significantly improved, with the optimal horn exhibiting a minimal frequency variation of 64 Hz compared to 90 Hz and 82 Hz for other samples. Hardness varies with tempering temperature, reaching a peak of over 39.3 HRC at 450°C and dropping to 23.8 HRC at 650°C. Microstructural analysis reveals transformations in pearlite, spheroidization, and increased grain sizes in the optimal sample. Carbide precipitation is more pronounced in longitudinal sections and increases with higher tempering temperatures and soaking times. The presence of chromium alloying elements in SCM440 steel contributes to carbide formation. These findings underscore the critical role of heat treatment conditions in optimizing the performance of ultrasonic horns.

KEYWORDS

heat treatment, ultrasonic horns, quenching and tempering, SCM440 steel, microstructural analysis

1 Introduction

Advanced technology is evolving rapidly due to new materials and improvements in traditional ones (Papadakis, 1984; Toozandehjani et al., 2015). These innovative materials have exceptional properties, which can be harnessed efficiently through mechanical joining processes. To achieve this across various materials, it is crucial to use methods that reduce excess heat while maintaining joint quality. This boosts production efficiency and enhances final product quality.

Ultrasonic technology has emerged as a prominent choice within various technology-driven industries, taking the forefront in technological innovations. Ultrasonic vibrations have been extensively applied to a diverse range of mechanical joining processes, including ultrasonic plastic welding (Nguyen et al., 2020; Nguyen H. T. et al., 2021), ultrasonic-assisted welding (Kumar et al., 2017; Cheng et al., 2022; Fan et al., 2023), ultrasonic-assisted

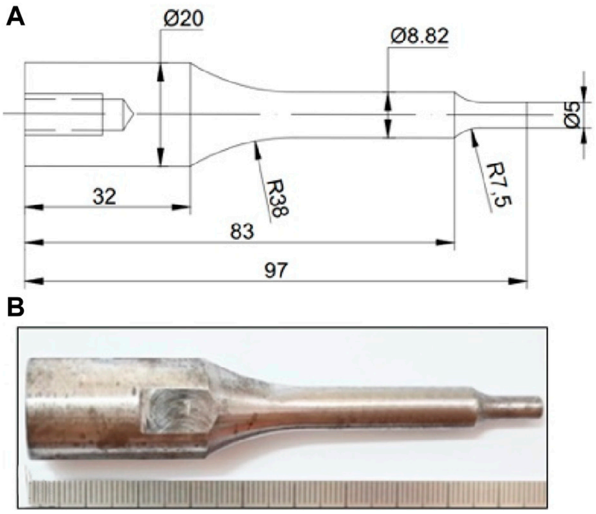

FIGURE 1
Ultrasonic welding horn of 28 kHz before heat treatment: **(A)** 2D model, **(B)** fabricated component.

TABLE 1 The elemental composition of the specimens.

C	Mn	Si	Cr	Mo	Ni
0.383	0.774	0.276	1.143	0.198	0.034

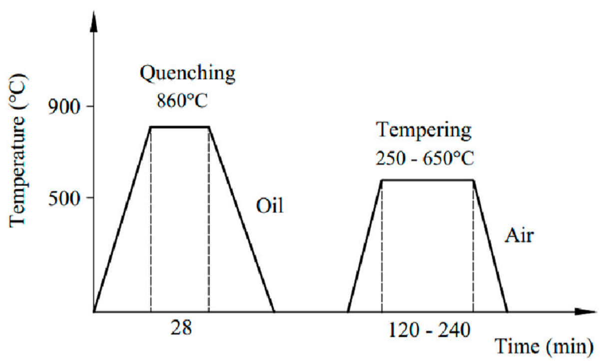

FIGURE 2
A schematic representation of SCM440 steel heat treatments.

clinching (Nanaumi et al., 2014; Merklein et al., 2023) and ultrasonic-assisted bonding (Wang et al., 2021). Ultrasonic-assisted welded joints show the highest mechanical integrity, followed by ultrasonic bonding as the second-best option, while ultrasonic-assisted riveting performs less effectively (Ding and Wu, 2019). Within the realm of welding, ultrasonic technology falls under the category of solid-state welding methods, encompassing techniques such as ultrasonic-assisted friction stir welding (Ni et al., 2020; Zhao et al., 2021; Wu et al., 2022; Muhammad et al., 2023), ultrasonic spot welding (Ni and Ye, 2018; Chung et al., 2022), and ultrasonic arc welding (Era et al., 2009; Wang et al., 2020).

Moreover, ultrasonic-assisted Metal Inert Gas (MIG) welding has gained substantial popularity in the welding domain, particularly due to its applicability to both non-ferrous alloy and ferrous alloy metals. Extensive research has been conducted on MIG, highlighting its ability to reduce spatter (Xie et al., 2020), influence microstructure (Jose et al., 2016; Liu et al., 2017), and improve the mechanical characteristics of welded joints (Watanabe et al., 2010; Shu et al., 2012; Huang et al., 2019). The ultrasonic horn, also known as the sonotrode, assumes a pivotal role within ultrasonic welding equipment, directly impacting the quality and efficiency of the machining process (Nguyen et al., 2017). The design of the acoustic horn holds paramount significance in determining the overall quality and efficiency of machining (Nad, 2011). Typically, sonotrodes are constructed from materials with high fatigue strengths and low acoustic losses (Gür and Tuncer, 2005a). Among the materials commonly employed for ultrasonic horns, steel, titanium alloy, and aluminum alloy stand out. Steel, in particular, exhibits substantial potential for enhancing the performance of ultrasonic horns. However, the widely adopted heat treatment processes in manufacturing industries, aimed at bolstering the mechanical properties of steel, can inadvertently alter the sound wave propagation characteristics of heat-treated steel (Prasad and Kumar, 1994b; Bongyoung and Seung Seok, 2000; Spindola and Buono, 2020). Therefore, to ensure the desired mechanical properties and efficient sound wave transmission, materials used in the production of ultrasonic horns must undergo rigorous verification.

The interaction between bulk materials and ultrasonic waves has garnered significant attention in the field of material characterization. Ultrasonic waves, as they propagate through polycrystalline materials, disperse at grain boundaries, leading to phenomena such as scattering, reflection, energy loss, and attenuation. Wave speed and energy losses due to microstructure interactions are key factors in ultrasonic material characterization (Gur and Keleş, 2003; Gür and Tuncer, 2004). Researchers have

TABLE 2 Factors and levels in the DOE.

Factor	Code and unit of factors	Levels		
		Level- 1	Level 0	Level +1
Tempering temperature	x_1(°C)	250	450	650
Soaking time during tempering	x_2(min)	120	180	240

TABLE 3 The array of heat treatment processes.

Sample no.	Quenching		Tempering	
	Temp. (°C)	Soaking time (min)	Temp. (°C)	Soaking time (min)
1	860	28	250	120
2	860	28	250	120
3	860	28	250	240
4	860	28	450	240
5	860	28	450	180
6	860	28	450	180
7	860	28	650	120
8	860	28	650	240
9	860	28	650	180

TABLE 4 Design matrix for the mechanical quality factors Q_m.

Run order	x_1	x_2	Exper. Q_m	Predicted Q_m	Residual
1	−1	−1	2,408	2391.00	17.00
2	+1	−1	4428	4396.00	32.00
3	−1	+1	2,939	2,873.67	65.33
4	+1	+1	4959	4878.67	80.33
5	−1	0	2,550	2,632.33	−82.33
6	+1	0	4525	4637.33	−112.33
7	0	−1	4677	4650.67	26.33
8	0	+1	5063	5133.33	−70.33
9	0	0	4936	4892.00	44.00

TABLE 5 Analysis of variance for the mechanical quality factors Q_m.

Source	DF	Adj SS	Adj MS	F-value	*p*-value
Model	5	9,551,774	1,910,355	207.21	0.001
Linear	2	6,379,488	3,189,744	345.98	0.000
x_1	1	6,030,037	6,030,037	654.05	0.000
x_2	1	349,451	349,451	37.90	0.009
Square	2	3,172,286	1,586,143	172.04	0.001
x_1*x_1	1	3,160,936	3,160,936	342.85	0.000
x_2*x_2	1	11,350	11,350	1.23	0.348
2-Way Interaction	1	0	0	0.00	1.000
x_1*x_2	1	0	0	0.00	1.000
Error	3	27,658	9,219		
Total	8	9,579,433			

diligently explored the correlation between ultrasonic wave transmission and several material characteristics, including microstructure, particle morphology, phase transformation, and the elastic modulus of individual grains. For example, Nguyen et al. (Nguyen T.-H. et al., 2021) conducted an investigation on 20CrMo ultrasonic horns, studying the influence of heat treatment on their performance by subjecting the horns to various tempering temperatures and soaking times, consequently observing changes in mechanical properties and sound wave transmission efficiency. Similarly, Gür and Tuncer (Gür and Tuncer, 2005b) explored phase transformation effects on sound velocity in AISI 4140 and AISI 5140 steels, revealing distinct wave velocity sequences in various steel phases. Keran et al. (Keran et al., 2017) explored the relationship between wave propagation direction, sound velocity, and grain orientation in cold-extruded aluminum samples, underscoring the profound impact of grain orientation on sound velocity and thus emphasizing the pivotal role of material microstructure in ultrasonic behavior. Aghaie-Khafri et al. (Aghaie-Khafri et al., 2012) investigated the interplay between ultrasonic attenuation, microstructure, and mechanical properties in AISI 301 stainless steel, revealing a direct correlation between annealing temperature, grain size, and mechanical properties. Additionally, Prasad and Kumar (Prasad and Kumar, 1994a) investigated longitudinal ultrasonic velocity and attenuation in cast steel post-deformation and various thermal treatments, detailing tempering's impact on sound properties. Furthermore,

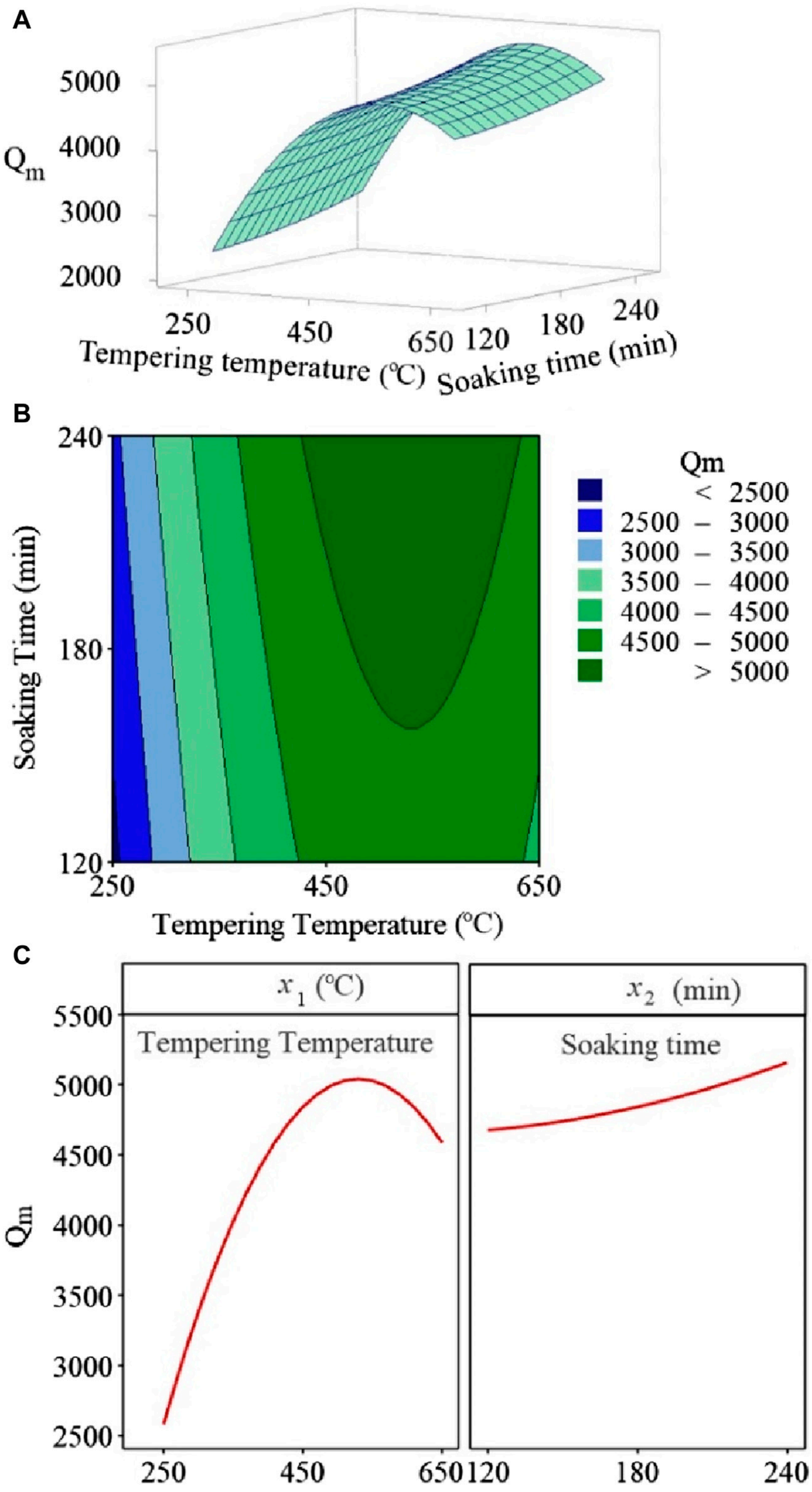

FIGURE 3
Plots of Q_m, termpering temperature and soaking time: **(A)** suface, **(B)** contour and **(C)** main effects.

Chaudhary and Sinha (Chaudhary and Sinha, 2008) delved into the velocity and attenuation properties in medium carbon steels, observing an increase in plastic deformation with the growing misorientation of recrystallized grains. Moreover, ultrasonic attenuation increased with the increasing interlamellar spacing of ferrite in pearlite, as well as the volume of ferrite. Zhu et al. (Zhu et al., 2019) carried out a comprehensive investigation into the microstructure of 9Cr-1Mo heat-resistant steel during creep processes involving ultrasonic parameters. Throughout the deformation procedures, ultrasonic attenuation exhibited a close

TABLE 6 Model Summary after eliminating the non-significant coefficients.

S	R-sq (%)	R-sq (adj) (%)	R-sq (pred) (%)
88.3274	99.59	99.35	98.76

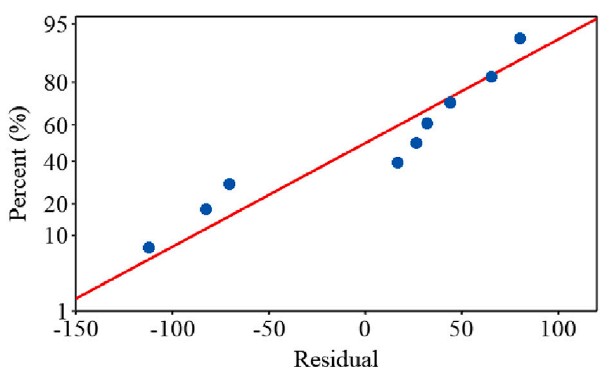

FIGURE 4
Normal distribution plot of residual values.

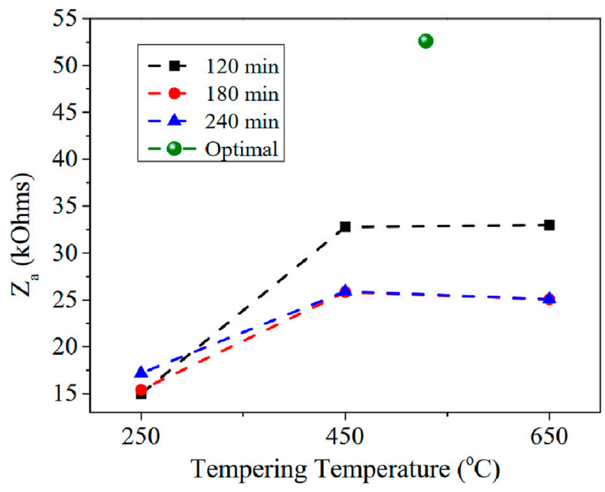

FIGURE 6
The impedance at the anti-resonance frequency of the heat-treated ultrasonic horns.

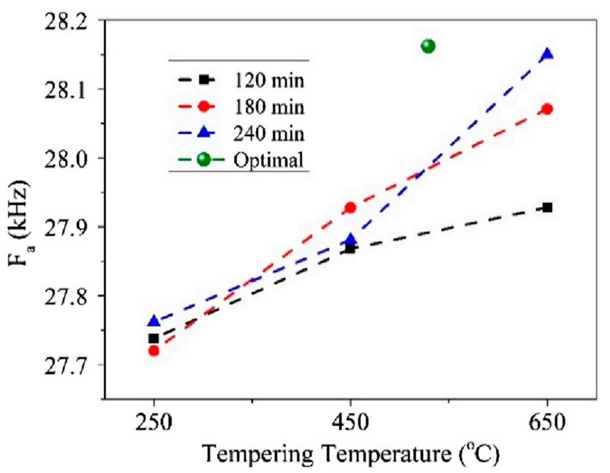

FIGURE 5
The anti-resonance frequency of the heat-treated ultrasonic horns.

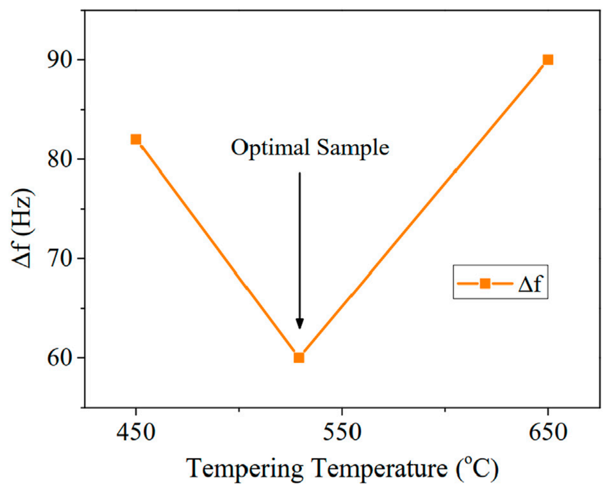

FIGURE 7
The frequency variation of specimens at various tempering temperatures for 240 min in 15 s.

correlation with the microstructure, particularly the dislocation damping arising from interactions between dislocations and precipitates. Precipitates, specifically carbides, underwent widening and coarsening as the precipitate average diameter increased, consequently fostering an increase in ultrasonic velocity.

The main goal of this study is to optimize the tempering temperature and soaking time parameters for SCM440 steel ultrasonic horns in the context of ultrasonic-assisted MIG welding. The research aims to significantly enhance the mechanical quality (Q_m) and frequency stability of ultrasonic horns. Additionally, the study seeks to investigate the microstructural changes responsible for these improvements and understand the influence of heat treatment factors on the behavior of ultrasonic horns. The outcomes of this study hold the potential to advance ultrasonic welding technology and contribute to the design and production of ultrasonic horns with enhanced properties, catering to various industrial applications.

2 Materials and methods

2.1 Materials

In this study, an ultrasonic horn operating at a frequency of 28 kHz was designed and fabricated, Figure 1. This horn can be used to investigate the penetration of ultrasonic vibration on MIG welding [15)]. The chemical formulation of SCM440 in this experiment was shown in Table 1.

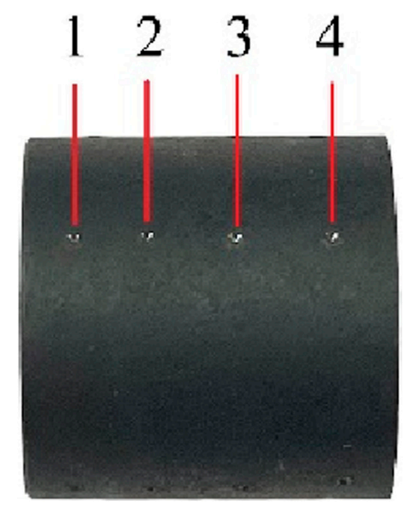

FIGURE 8
Locations for measuring hardness on the cylindrical test specimen.

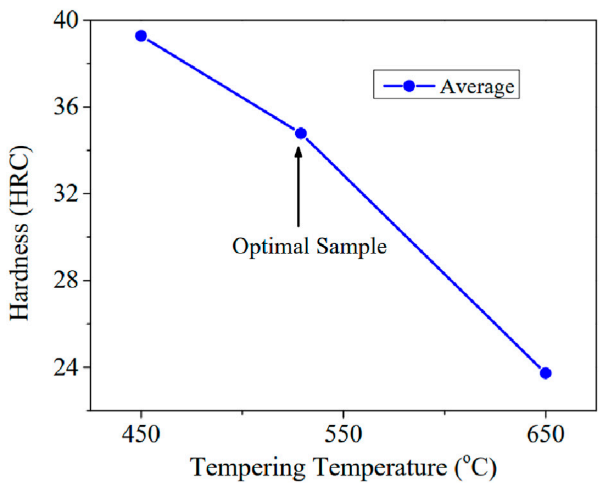

FIGURE 9
The average hardness of heat-treated horn after different tempering temperatures for 240 min.

2.2 Design of the experiment and the heat treatment processes

DOE (Design of Experiments) is a powerful method using mathematical models to solve process issues. Response Surface Methodology (RSM) is a statistical approach that assesses the effects of factors, aiming to optimize a specific response, either a maximum or minimum value. In this study, RSM is used to find the best heat treatment process to optimize Q_m, a vital parameter for ultrasonic horns, where damping is inversely related to Q_m. Orthogonal-Array Composite Designs (OACDs) with 2 factors, each having 3 levels, and a total of 9 experiments are utilized, Table 2. The optimization parameters are tempering temperature x_1 and soaking time during tempering x_2. The regression equation is for estimating the dependent variable Y, known as the response with the independent variables x_1 and x_2. The regression equation can be written as:

$$Y = a_0 + a_1x_1 + a_2x_2 + a_{12}x_1x_2 + a_{11}x_1^2 + a_{22}x_2^2$$

Where a_1, a_2, a_{11}, a_{22} were the coefficients to represent the effect of each factor x_1 and x_2. The a_{12} was the coefficient to represent the effect of the interaction between the factor x_1 and x_2.

The specimens were raised to the austenitizing temperature of 860°C and subsequently immersed in oil for quenching. The approximate soaking duration, calculated considering the carbon weight percentage, sample shape, and thickness, was 28 min. Tempering processes were conducted at three distinct temperatures: 250°C for 120 min, 450°C for 180 min, and 650°C for 240 min. Afterward, the samples were air-cooled, Figure 2. A comprehensive list of these processes can be found in Table 3.

After completing all heat treatment processes, the ultrasonic horns underwent testing using the TRZ Analyzer to collect Q_m values, which served as the outcome variables.

3 Results and discussion

3.1 Analysis of the established model

After conducting the experimental procedures, data is gathered and analyzed using MINITAB® version 21 software to assess the coefficients of the second-level regression equation and optimize the regression function. Table 4 displays the experimental values, predicted values, and residuals, which indicate the reliability of the mathematical model.

Comparison of the *p*-values to the significant level that removes the non-significant regression coefficient. At the significance level $p = 0.05$, the values a_{22} ($p = 0.348$) and a_{12} ($p = 1.00$) are rejected because the *p*-value of its coefficient is greater than 0.05, Table 5. The significance of factors on the response, including tempering temperature and soaking time during tempering, is evident due to *p*-values below 0.05. It is notable that the linear aspects of tempering temperature and soaking time during tempering, along with the squared tempering temperature term, are correlated with mechanical quality, Figure 3. Therefore, the mechanical quality will improve when these variables are increased. The values of R^2 (99.59%) and R^2 (adj) (99.35%) indicate that the regression model determines a high correlation between the actual and predicted values of the response, Table 6.

OACDs maintain coefficient independence, permitting the removal of non-significant coefficients without recomputing the regression equation. This leads to the following regression function in uncoded units after eliminating the non-significant coefficients.

$$Y(Q_m) = -4452 + 33.30x_1 + 4.022x_2 - 0.03143x_1 \times x_1$$

The experimental model needs validation for theoretical model reliability under various conditions and at the optimal condition.

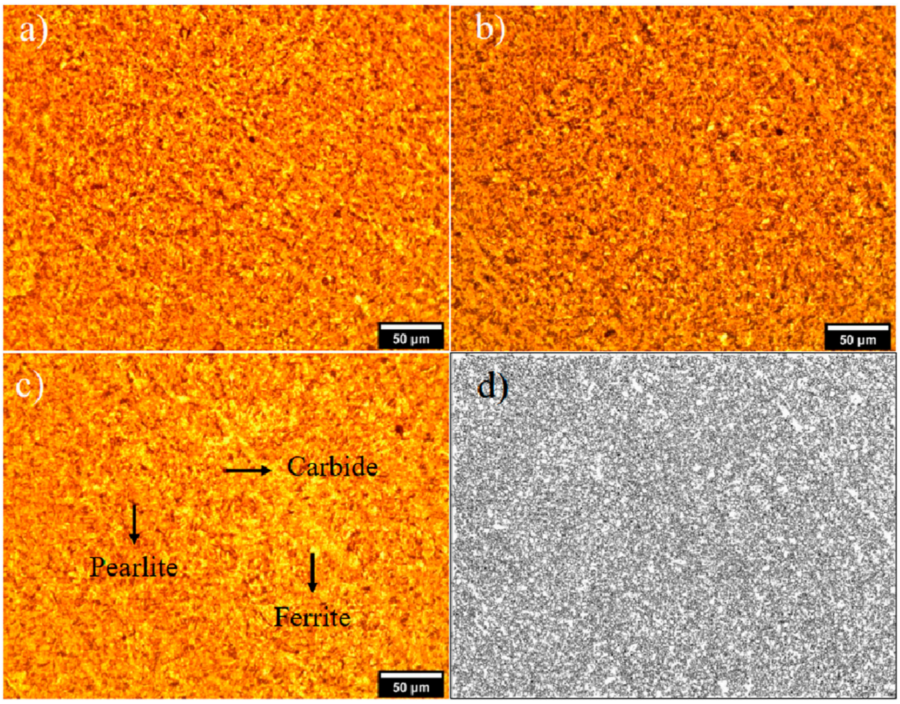

FIGURE 10
Microstructure of sample No. 8 of the cross-section: **(A)** c_1, **(B)** c_2, **(C)** c_3 and **(D)** 400 × image processed using ImageJ application.

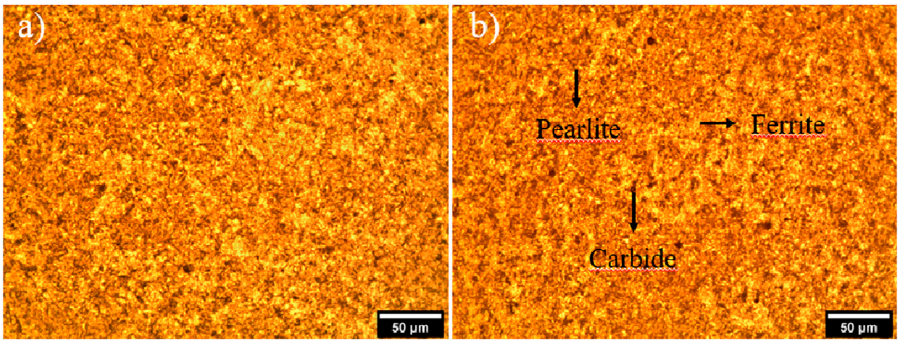

FIGURE 11
Microstructure of sample No. 8 of the longitudinal section: **(A)** l_1, **(B)** l_2.

Instead of using Chi-Square, model compatibility is evaluated by calculating the experimental error between theoretical and experimental values. A normal probability plot of residuals is used to confirm normally distributed residuals, where residual points create an almost straight line, Figure 4.

Based on the regression equation, the ideal conditions are at a tempering temperature of 529°C for 240 min. The experimental and predicted values under these optimal conditions are 5430 and 5358.3 for the mechanical quality factor Q_m. The experimental error is 1.3%, indicating a relatively consistent difference between theory and actual values.

3.2 Horn analysis

The key parameters in the ultrasonic welding system include the anti-resonance frequency (F_a) and its corresponding impedance (Z_a) at F_a. Z_a exhibits its maximum electrical impedance modulus at F_a, leading to minimal current demand on the generator. Figure 5 displays the anti-resonance frequencies of heat-treated ultrasonic horns, with samples under optimal conditions at 529°C/240 min having the highest F_a value. The F_a value increases with longer soaking times. Figure 6 depicts the impedance at the anti-resonance

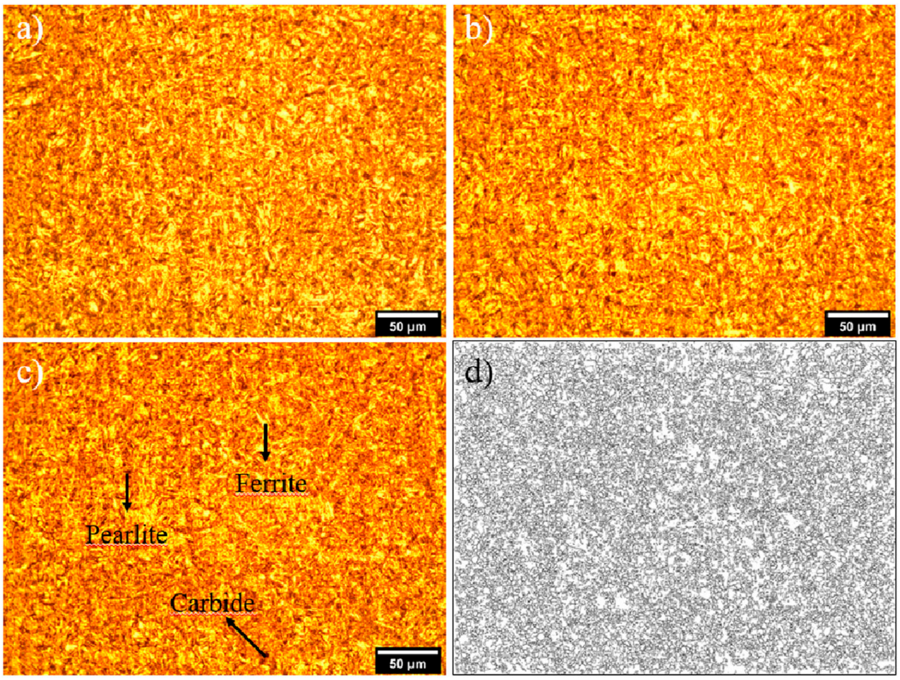

FIGURE 12
Microstructure of optimal sample of the cross-section: **(A)** c_1, **(B)** c_2, **(C)** c_3 and **(D)** 400 × image processed using ImageJ application.

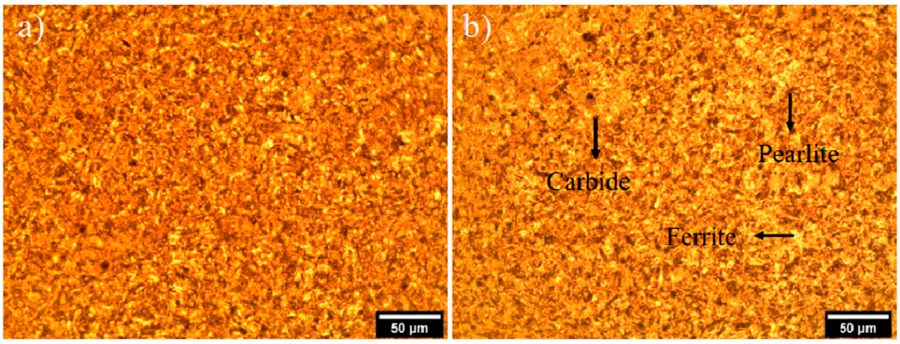

FIGURE 13
Microstructure of optimal sample of the longitudinal section: **(A)** l_1, **(B)** l_2.

frequency of the heat-treated ultrasonic horns. At a constant soaking time of 240 min, higher tempering temperatures result in higher Z_a values. Samples in the optimal conditions of 529°C/240 min have the highest Z_a value.

3.3 Frequency in working condition

The horn is attached to the ultrasonic system and operated for 15 s to assess frequency variations. The experiment uses three high-Q_m ultrasonic horns: No. 4 (650°C), No. 8 (450°C), and the optimal sample (529°C) in 240 min. In Figure 7, during a welding time of 15 s, the optimal ultrasonic horn (529°C/240 min) exhibits the minimum frequency variation of Δf = 64 Hz, which is lower than that of sample No. 4 (Δf = 90 Hz) and sample No. 8 (Δf = 82 Hz).

3.4 Hardness measurement

The specimens are tested on the C scale with a diamond indenter and subjected to a 1.5 kN load for 10 s. Measurements are taken at four positions on the surface of those specimens, spaced 2–4 mm apart, Figure 8.

The tempering temperature increases, while keeping the soaking time constant, the hardness values gradually decrease. The average hardness reaches its maximum at over 39.3 HRC when tempering at a medium temperature of 450°C. However, when the temperature is raised to 650°C, it decreases significantly to only 23.8 HRC, Figure 9.

3.5 Microstructure

To examine the microstructure, the horn is cut both longitudinally and transversely. In the transverse cross-section,

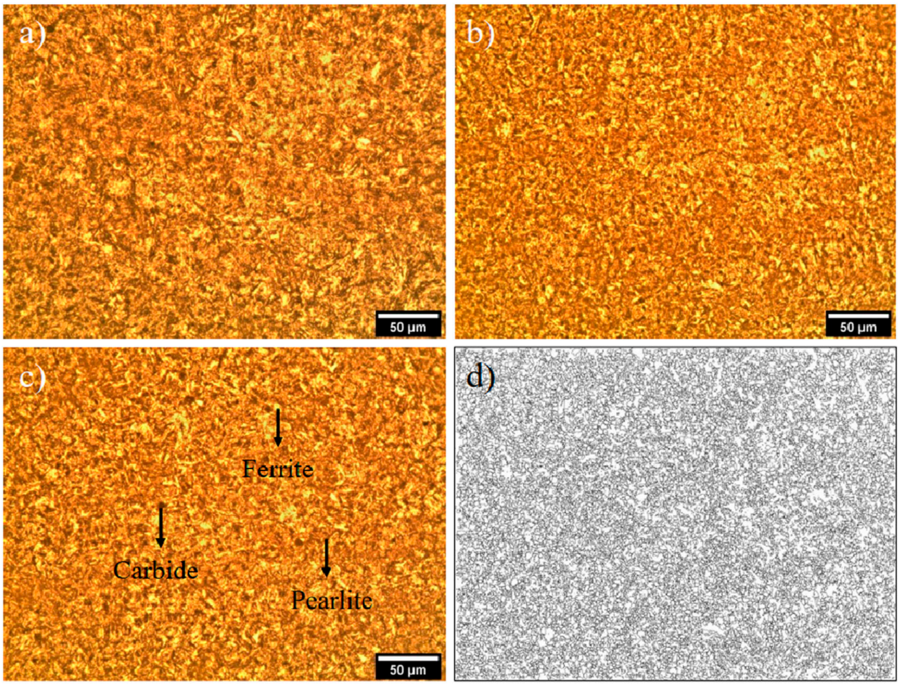

FIGURE 14
Microstructure of sample No. 4 of the cross-section: **(A)** c_1, **(B)** c_2, **(C)** c_3 and **(D)** 400 × image processed using ImageJ application.

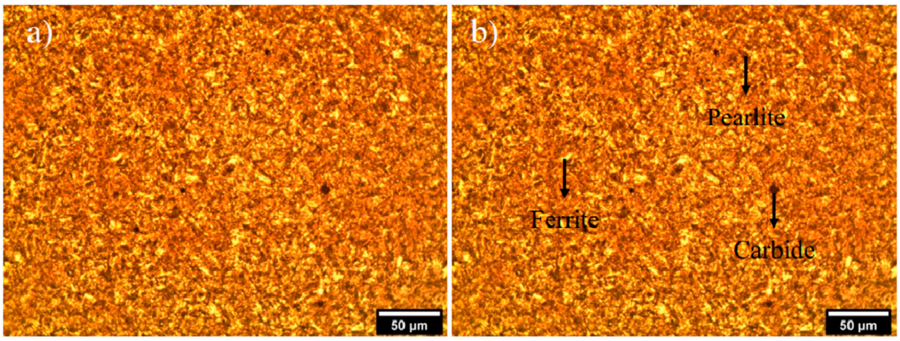

FIGURE 15
Microstructure of sample No. 4 of the longitudinal section: **(A)** l_1, **(B)** l_2.

three positions are examined: right at the center (c_1), 3 mm from the center towards the edge (c_2), and 2 mm from the edge (c_3). In the longitudinal direction, measurements are taken right at the center (l_1) and at a second point 3 mm away from the first point (l_2).

Figure 10 to Figure 15 depict the microstructures of the No. 8, No. 4 and optimal samples. Both the longitudinal and cross sections at a temperature of 450°C/240 min show that the shape of pearlite is similar to needle-like martensite, but with slightly rounded tips, Figure 10 and Figure 11. The spheroidization of pearlite involves the transformation of the shape of the cementite lamellae into a spherical one, Figure 12 and Figure 13. The results of the spherical transformation are most apparent in Figure 14 and Figure 15. Sufficient time for the transformation phase allows for the increase in grain size of pearlite. After processing the images using the ImageJ application, we determined the quantities and average sizes of grains in the microstructures, Table 7. For sample No. 8, the average size of 25,214 grains was 1.727 μm^2, (Figure 10D). In the optimal sample, the average size of 15,417 grains was 2.66 μm^2, (Figure 12D). Additionally, in sample No. 4, the average size of 13,965 grains was 3.251 μm^2, (Figure 14D). The SCM440 steel contains chromium elements. It is evident that these are carbides formed due to the Cr alloying element. In the longitudinal sections of all three samples, the microstructure shows more pronounced carbide precipitation with larger sizes compared to the cross-sections. Increasing the tempering temperature and extending the soaking time result in an increased number and

TABLE 7 The total number of grains and the average cementite grains size processed by ImageJ application.

Sample	Count gains	Average cementite gains (μm^2)
No. 8	25,214	1.727
Optimal sample	15,417	2.66
No. 4	13,965	3.251

size of carbides formed by alloying elements, Figure 11, Figure 13 and Figure 15.

4 Conclusion

This paper focuses on the heat treatment of ultrasonic horns through quenching and tempering processes to explore their impact and the interaction of heat treatment process parameters, particularly for SCM440 steel. The key findings are outlined as follows:

a. The study identified the optimal heat treatment conditions for ultrasonic horns as a tempering temperature of 529°C for 240 min, resulting in improved mechanical quality (Qm) with a 1.3% experimental error.
b. The optimal heat-treated ultrasonic horn exhibited the most stable frequency during welding, with a frequency variation of only 64 Hz, compared to 90 Hz and 82 Hz for other samples.
c. The hardness of the specimens decreased as the tempering temperature increased, with the maximum hardness of over 39.3 HRC observed at 450°C, but a significant drop to 23.8 HRC at 650°C.
d. Microstructural analysis revealed the transformation of pearlite and spheroidization, with increased grain sizes in the optimal sample. Carbide precipitation was more pronounced in longitudinal sections and increased with higher tempering temperatures and soaking times
e. The presence of chromium alloying elements in SCM440 steel was identified as contributing to the formation of carbides in the microstructure.

Data availability statement

The original contributions presented in the study are included in the article/supplementary material, further inquiries can be directed to the corresponding author.

Author contributions

VT: Conceptualization, Validation, Writing–original draft. TQ: Software, Writing–original draft. NN: Methodology, Writing–original draft. HT: Writing–original draft, Software. TK: Writing–original draft, Investigation. TN: Supervision, Writing–review and editing, Conceptualization.

Funding

The author(s) declare that financial support was received for the research, authorship, and/or publication of this article. This research was funded by Vietnam National University HoChiMinh City (VNU-HCM) under grant number: B2023-20-13.

Conflict of interest

The authors declare that the research was conducted in the absence of any commercial or financial relationships that could be construed as a potential conflict of interest.

Publisher's note

All claims expressed in this article are solely those of the authors and do not necessarily represent those of their affiliated organizations, or those of the publisher, the editors and the reviewers. Any product that may be evaluated in this article, or claim that may be made by its manufacturer, is not guaranteed or endorsed by the publisher.

References

Aghaie-Khafri, M., Honarvar, F., and Zanganeh, S. (2012). Characterization of grain size and yield strength in AISI 301 stainless steel using ultrasonic attenuation measurements. *J. Nondestruct. Eval.* 31 (3), 191–196. doi:10.1007/s10921-012-0134-z

Bongyoung, A., and Seung Seok, L. (2000). Effect of microstructure of low carbon steels on ultrasonic attenuation. *EEE Trans. Ultrason. Ferroelectr. Freq. Control* 47 (3), 620–629. doi:10.1109/58.842049

Chaudhary, S. K., and Sinha, V. K. (2008). Ultrasonic behavior of plastically deformed and heat treated steel. *Trans. Indian Inst. Mater.* 61 (2), 217–220. doi:10.1007/s12666-008-0033-2

Cheng, X. M., Yang, K., Wang, J., Xiao, W. T., and Huang, S. S. (2022). Ultrasonic system and ultrasonic metal welding performance: a status review. *J. Manuf. Process.* 84, 1196–1216. doi:10.1016/j.jmapro.2022.10.067

Chung, V.T.-T., Nguyen, T. C., Bui, D. K., Nguyen, H. L., Van Nguyen, A., and Nguyen, T.-H. (2022). Penetration and microstructure of steel joints by ultrasonic-assisted gas metal arc welding. *Jpn. J. Appl. Phys.* 61 (4), 046502. doi:10.35848/1347-4065/ac4d44

Ding, W., and Wu, C. (2019). Effect of ultrasonic vibration exerted at the tool on friction stir welding process and joint quality. *J. Manuf. Process.* 42, 192–201. doi:10.1016/j.jmapro.2019.04.026

Era, T., Ueyama, T., and Hirata, Y. (2009). Spatter reduction in gas metal arc welding of stainless steel sheets using controlled bridge transfer process. *Sci. Technol. Weld.* 14 (8), 708–716. doi:10.1179/136217109X12518083193595

Fan, Z., Bai, K., and Chen, C. (2023). The application of ultrasound in Joining: principles, processes and properties. *J. Manuf. Process.* 101, 269–299. doi:10.1016/j.jmapro.2023.05.094

Gür, C., and Tuncer, B. (2004). "Investigating the microstructure-ultrasonic property relationships in steels," in World Conf. on NDT, Canada.

Gür, C. H., and Tuncer, B. O. (2005a). Characterization of microstructural phases of steels by sound velocity measurement. *Mat. Charact.* 55 (2), 160–166. doi:10.1016/j.matchar.2005.05.002

Gür, C. H., and Tuncer, B. O. (2005b). Characterization of microstructural phases of steels by sound velocity measurement. *Mater. Charact.* 55 (2), 160–166. doi:10.1016/j.matchar.2005.05.002

Gur, H., and Keleş, Y. (2003). Ultrasonic characterisation of hot-rolled and heat-treated plain carbon steels. *Insight non-destr. Test. Cond.* 45, 615–620. doi:10.1784/insi.45.9.615.52936

Huang, L., Hua, X., Wu, D., Jiang, Z., and Ye, Y. (2019). A study on the metallurgical and mechanical properties of a GMAW-welded Al-Mg alloy with different plate thicknesses. *J. Manuf. Process.* 37, 438–445. doi:10.1016/j.jmapro.2018.12.017

Jose, M. J., Kumar, S. S., and Sharma, A. (2016). Vibration assisted welding processes and their influence on quality of welds. *Sci. Technol. Weld.* 21 (4), 243–258. doi:10.1179/1362171815Y.0000000088

Keran, Z., Mihaljević, M., Runje, B., and Markučič, D. (2017). Ultrasonic testing of grain distortion direction in cold formed aluminium profile. *Arch. Civ. Mech. Eng.* 17 (2), 375–381. doi:10.1016/j.acme.2016.11.003

Kumar, S., Wu, C. S., Padhy, G. K., and Ding, W. (2017). Application of ultrasonic vibrations in welding and metal processing: a status review. *J. Manuf. Process.* 26, 295–322. doi:10.1016/j.jmapro.2017.02.027

Liu, C., Chen, D., Hill, M. R., Tran, M. N., and Zou, J. (2017). Effects of ultrasonic impact treatment on weld microstructure, hardness, and residual stress. *Mat. Sci. Technol.* 33 (14), 1601–1609. doi:10.1080/02670836.2017.1299277

Merklein, M., Jäckisch, M., Kuball, C.-M., Römisch, D., Wiesenmayer, S., and Wituschek, S. (2023). Mechanical joining of high-strength multi-material systems – trends and innovations. *Mech. Ind.* 24, 16. doi:10.1051/meca/2023013

Muhammad, N. A., Geng, P., Wu, C., and Ma, N. (2023). Unravelling the ultrasonic effect on residual stress and microstructure in dissimilar ultrasonic-assisted friction stir welding of Al/Mg alloys. *Int. J. Mach. Tools Manuf.* 186, 104004. doi:10.1016/j.ijmachtools.2023.104004

Nad, M. (2011). Ultrasonic horn design for ultrasonic machining technologies. *J. Appl. Comput. Mech.* 4, 79–88.

Nanaumi, G., Mizushima, D., and Ohtake, N. (2014). Joining of various kinds of metal plates using ultrasonic vibrations. *Procedia Eng.* 81, 2111–2116. doi:10.1016/j.proeng.2014.10.294

Nguyen, H. T., Le, T. Q., Nguyen, L. H., and Truong, K. D. (2021a). Design of a radial ultrasonic horn for plastic welding using finite element analysis. *Jpn. J. Appl. Phys.* 60 (9), 096502. doi:10.35848/1347-4065/ac1ecf

Nguyen, T.-H., Nguyen, L. T., Quynh Tran, T. M., Nguyen, N. H., and Chung, V.T.-T. (2021b). Analysis of process parameters of hypoeutectoid steel ultrasonic horns with different heat treatment processes. *Jpn. J. Appl. Phys.* 60 (12), 126502. doi:10.35848/1347-4065/ac3727

Nguyen, T. H., Quang, Q. T., Tran, C. L., and Nguyen, H. L. (2017). Investigation the amplitude uniformity on the surface of the wide-blade ultrasonic plastic welding horn. *IOP Conf. Ser. Mat. Sci. Eng.* 241, 012023. doi:10.1088/1757-899x/241/1/012023

Nguyen, T.-h., Thanh, L. Q., Loc, N. H., Huu, M. N., and Nguyen Van, A. (2020). Effects of different roller profiles on the microstructure and peel strength of the ultrasonic welding joints of nonwoven fabrics. *Appl. Sci.* 10 (12), 4101. doi:10.3390/app10124101

Ni, Z. L., Yang, J. J., Hao, Y. X., Chen, L. F., Li, S., Wang, X. X., et al. (2020). Ultrasonic spot welding of aluminum to copper: a review. *Int. J. Adv. Manuf. Technol.* 107 (1), 585–606. doi:10.1007/s00170-020-04997-5

Ni, Z. L., and Ye, F. X. (2018). Ultrasonic spot welding of aluminum alloys: a review. *J. Manuf. Process.* 35, 580–594. doi:10.1016/j.jmapro.2018.09.009

Papadakis, E. J. I. M. R. (1984). Physical acoustics and microstructure of iron alloys. *Int. Mat. Rev.* 29 (1), 1–24. doi:10.1179/095066084790149147

Prasad, R., and Kumar, S. (1994a). Study of the influence of deformation and thermal treatment on the ultrasonic behaviour of steel. *J. Mat. Process. Tech.* 42 (1), 51–59. doi:10.1016/0924-0136(94)90074-4

Prasad, R., and Kumar, S. (1994b). Study of the influence of deformation and thermal treatment on the ultrasonic behaviour of steel. *J. Mat. Process. Tech.* 42, 51–59. doi:10.1016/0924-0136(94)90074-4

Shu, K. M., Hsieh, W. H., and Chi, C. W. (2012). On the design and analysis of acoustic horns for ultrasonic welding. *Adv. Mat. Res.* 472-475, 1555–1558. doi:10.4028/www.scientific.net/AMR.472-475.1555

Spindola, M. O., and Buono, V. T. L. (2020). Effect of intercritical annealing with high cooling rate associated with cold deformation and subcritical annealing on microstructure and mechanical properties of SAE 52100. *J. Mat. Res. Tech.* 9 (4), 9136–9141. doi:10.1016/j.jmrt.2020.05.106

Toozandehjani, M., Matori, K. A., Ostovan, F., Mustapha, F., Zahari, N. I., and Oskoueian, A. J. J. o.M. S. (2015). On the correlation between microstructural evolution and ultrasonic properties: a review. *J. Mat. Sci.* 50, 2643–2665. doi:10.1007/s10853-015-8855-x

Wang, H., Tong, X., Chen, Y., Hua, L., Wu, M., and Ji, W. (2021). Study on ultrasonic vibration-assisted adhesive bonding of CFRP laminates with laser ablation-treated surfaces. *Compos. Struct.* 268, 113983. doi:10.1016/j.compstruct.2021.113983

Wang, Y., Yu, C., Lu, H., and Chen, J. (2020). Research status and future perspectives on ultrasonic arc welding technique. *J. Manuf. Process.* 58, 936–954. doi:10.1016/j.jmapro.2020.09.005

Watanabe, T., Shiroki, M., Yanagisawa, A., and Sasaki, T. (2010). Improvement of mechanical properties of ferritic stainless steel weld metal by ultrasonic vibration. *J. Mat. Process. Tech.* 210 (12), 1646–1651. doi:10.1016/j.jmatprotec.2010.05.015

Wu, C., Wang, T., and Su, H. (2022). Material flow velocity, strain and strain rate in ultrasonic vibration enhanced friction stir welding of dissimilar Al/Mg alloys. *J. Manuf. Process.* 75, 13–22. doi:10.1016/j.jmapro.2021.12.055

Xie, W., Huang, T., Yang, C., Fan, C., Lin, S., and Xu, W. (2020). Comparison of microstructure, mechanical properties, and corrosion behavior of Gas Metal Arc (GMA) and Ultrasonic-wave-assisted GMA (U-GMA) welded joints of Al–Zn–Mg alloy. *J. Mat. Process. Tech.* 277, 116470. doi:10.1016/j.jmatprotec.2019.116470

Zhao, W., Wu, C., and Shi, L. (2021). Acoustic induced antifriction and its effect on thermo-mechanical behavior in ultrasonic assisted friction stir welding. *Int. J. Mech. Sci.* 190, 106039. doi:10.1016/j.ijmecsci.2020.106039

Zhu, L., Liu, X., Fan, P., and Liu, J. (2019). A study of microstructure evolution during creep of 9Cr-1Mo steel using ultrasonic and hardness measurements. *J. Mat. Eng. Perf.* 28 (4), 2348–2355. doi:10.1007/s11665-019-03987-3